Emission cross sections for electron-impact-induced line radiation in the vuv from Ne, Ar, and Kr: Measurements and comparison with theory

Wolfgang Jans, Bernd Möbus, Michael Kühne, and Gerhard Ulm
Physikalisch-Technische Bundesanstalt, Abbestrasse 2-12, 10587 Berlin, Germany

Andreas Werner and Karl-Heinz Schartner
I. Physikalisches Institut der Justus-Liebig-Universität Gießen, Heinrich-Buff-Ring 16, 35392 Gießen, Germany

(Received 22 July 1996)

A set of 18 absolute cross sections for electron-impact-induced line radiation of Ne, Ar, and Kr in the spectral range between 46 and 100 nm was measured providing an accurate database for the use of an electron-impact excitation source as a source of calculable radiant flux. Unparalleled, low relative uncertainties, mostly below 4%, were achieved, mainly because the electron storage ring BESSY served as a primary standard source in the vuv to determine the responsivity of the spectrometer-detector system used for the cross-section measurements, and because a spinning rotor gauge was used as a secondary standard for the determination of the target gas density. A comparison of our cross-section data with published experimental and theoretical data is presented. [S1050-2947(97)06603-1]

PACS number(s): 32.70.−n

I. INTRODUCTION

Electron-impact ionization is a fundamental process in atomic and molecular physics. The observation of electron-impact-induced line radiation provides detailed information on the excitation or the ionization and excitation process. Experimental cross-section data with low uncertainties are important to test the accuracy of theoretical descriptions of the electron-atom interaction and, moreover, they play an important role as basic data for the modeling of discharges, plasmas, controlled nuclear fusion, and planetary and stellar atmospheres.

Besides this fundamental interest, photoemission cross sections with small uncertainties are needed when electron-impact excitation sources are to be used as radiometric standards. Over the past years, interest in vacuum ultraviolet (vuv) spectroscopy has been steadily growing in atomic and molecular physics, surface and solid-state physics, but also in research areas such as controlled nuclear fusion and astrophysics. One of the basic requirements for a quantitative application of vuv spectroscopy is the availability of suitable radiometric standards.

In the spectral range of the vuv, electron storage rings have been proven to be reliable and accurate primary standard sources [1–3] with calculable synchrotron radiation (SR) emission. But as access to storage ring facilities will always be limited and as many radiometric calibrations have to be performed at the user's location, other standard sources are required. In the radiometry laboratory of the Physikalisch-Technische Bundesanstalt (PTB) at the electron storage ring BESSY in Berlin, different sources have been investigated [4], one of them being an electron-impact-excitation source [5].

This source is based on the electron-impact-induced line radiation from atoms and molecules [6–8]. Once the photoemission cross section $\sigma(\lambda_{jk},E)$ for an emission at wavelength λ_{jk} at the excitation energy E and the source parameters are known, in contrast to other sources and similar to an electron storage ring, an electron-impact excitation source is a ''source of calculable radiant flux'' and need not be calibrated. The electron-impact excitation source is a compact and low power-consuming source. It offers the opportunity of an optimal adaptation to the user's experiment and of *in situ* calibrations of spectrometer-detector systems.

Over 500 cross sections for electron-impact-induced transitions in the wavelength region from 25 to 200 nm for a variety of atomic and molecular targets were measured, demonstrating the large interest in these data. Unfortunately, most of them are known with a relative uncertainty $\Delta\sigma(\lambda_{jk},E)/\sigma(\lambda_{jk},E)$ of only 25%–50% [9]. These considerable uncertainties are predominantly caused by the lack of a primary standard source necessary for the determination of the responsivity of the spectrometer-detector system used for the photoemission cross-section measurements. The second main source of uncertainty is the determination of the target gas density. As a result of these problems, almost all published cross sections are based on relative measurements combined with normalization procedures. In many cases, theoretical results from the application of the first Born or Bethe approximation were used either directly or indirectly.

Up to now, the only photoemission cross-section measurements based on an absolute determination of all necessary parameters, especially on the absolute determination of the responsivity of the spectrometer-detector system used, were performed by Risley and co-workers [10–12] and by ourselves ([5], [13], and this work). Both groups used an electron storage ring as the primary standard source in the vuv to determine the responsivity of their spectrometer-detector system, but particularly differ in the illumination of their spectrometer grating. Moreover, they used different electron excitation energies and different means to determine the target gas density. So far, we concentrated on the determination of the emission cross section of the Ar II $3s3p^6\ ^2S_{1/2}$-$3s^23p^5\ ^2P_{3/2}$ transition at 91.98 nm [5] and found excellent agreement with the cross-section value determined by McPherson [9,10].

In this paper we present a set of 18 photoemission cross sections for lines in the wavelength range from 46 to 100 nm for the target gases Ne, Ar, and Kr at excitation energies of 2 and 3 keV. Since SR was used to determine the spectral responsivity of the monochromator-detector system and a spinning rotor gauge to determine the target gas density, unequalled, low relative uncertainties $\Delta\sigma(\lambda_{jk},E)/\sigma(\lambda_{jk},E)$, mostly below 4%, were achieved. (All uncertainties concerning our experiment are 1σ values.) The total relative uncertainty of the source parameters of the electron-impact excitation source of 1%, as described in [5], in combination with the accurate database of emission cross sections presented here demonstrates the excellent suitability of the electron-impact excitation source as a standard source in the vuv.

II. EXPERIMENTAL SETUP

A detailed description of the experimental setup, i.e., the electron-impact excitation source and the monochromator-detector system, the procedure for the determination of emission cross sections, and the achieved uncertainties was given recently [5,13]. Only a short description is provided here. The cross section for electron-impact-induced photoemission $\sigma(\lambda_{jk},E)$ is given by the electron beam of i/e electrons per second, the observed length ℓ of the electron beam, the target gas density n, and the radiant flux $\Phi^{\mathrm{SO}}(\lambda_{jk})$ emitted per second into a solid angle Ω. Because we always measured $\Phi^{\mathrm{SO}}(\lambda_{jk})$ perpendicular to the exciting electron beam ($\Theta=90°$), we determined the apparent cross section $\sigma_{\perp}(\lambda_{jk},E)$ according to Eq. (1), which is related to the emission cross section via Eq. (2) [9]:

$$\sigma_{\perp}(\lambda_{jk},E)=\frac{1}{n\ell\, i/e}\,\frac{4\pi}{\Omega}\,\Phi^{\mathrm{SO}}(\lambda_{jk}), \tag{1}$$

$$\sigma_{\perp}(\lambda_{jk},E)=f(P^{\mathrm{SO}}(\lambda_{jk}),\Theta)\sigma(\lambda_{jk},E), \tag{2}$$

where

$$f(P^{\mathrm{SO}}(\lambda_{jk}))=\frac{1-P^{\mathrm{SO}}(\lambda_{jk})\,\cos^2(\Theta)}{1-\frac{1}{3}\,P^{\mathrm{SO}}(\lambda_{jk})}.$$

Transitions with the upper level's total momentum $J<1$ emit isotropically, i.e., the degree of polarization of the radiation emitted by the source $P^{\mathrm{SO}}(\lambda_{jk})=0$ and $\sigma(\lambda_{jk},E)=\sigma_{\perp}(\lambda_{jk},E)$.

$\Phi^{\mathrm{SO}}(\lambda_{jk})$ was measured at the normal incidence monochromator beamline [14] in the PTB's radiometry laboratory at the electron storage ring BESSY. At this beamline, the spectrometer-detector system consists of a flux-limiting aperture (defining the solid angle of the accepted radiation), a concave imaging mirror, a 1-m normal incidence 15° McPherson-type monochromator, and a multiplier (Balzers SEV 217) behind the exit slit. An Os-coated ruled concave grating (2400 grooves/mm, blazed at 80 nm) was used throughout the experiments. Three differently coated (Au, SiC, Os) imaging mirrors were used to optimize the system's reflectivity and second-order suppression.

The entire spectrometer-detector system can be turned about a vertical axis to image either the tangent point of the storage ring or the electron beam of the electron-impact excitation source into the monochromator entrance slit. The latter measurements yield the count rate $i^{\mathrm{SO}}(\lambda_{jk})$. Observing the calculable spectral photon flux of a BESSY bending magnet $\Phi_{\lambda}^{\mathrm{SR}}(\lambda)$, two measurements must be performed with the optical plane of the spectrometer-detector system parallel and perpendicular to the electron orbit plane, leading to the count rates $i_0^{\mathrm{SR}}(\lambda)$ and $i_{90}^{\mathrm{SR}}(\lambda)$, respectively. From these data the polarization property of the instrumentation $M(\lambda)$ and the spectral responsivity $\overline{s(\lambda)}$ for unpolarized radiation are calculated according to Eq. (3):

$$M(\lambda)=\frac{1}{P^{\mathrm{SR}}(\lambda)}\,\frac{i_0^{\mathrm{SR}}(\lambda)-i_{90}^{\mathrm{SR}}(\lambda)}{i_0^{\mathrm{SR}}(\lambda)+i_{90}^{\mathrm{SR}}(\lambda)},\quad \overline{s(\lambda)}=\frac{i_0^{\mathrm{SR}}(\lambda)+i_{90}^{\mathrm{SR}}(\lambda)}{2\Phi_{\lambda}^{\mathrm{SR}}(\lambda)\Delta\lambda}. \tag{3}$$

$P^{\mathrm{SR}}(\lambda)$ is the calculated degree of polarization of the SR. $\Delta\lambda$ is the spectral bandwidth of the instrumentation. $\Phi^{\mathrm{SO}}(\lambda_{jk})$ follows according to Eq. (4):

$$\Phi^{\mathrm{SO}}(\lambda_{jk})=\frac{i^{\mathrm{SO}}(\lambda_{jk})}{\overline{s(\lambda_{jk})}}\,\frac{1}{1+P^{\mathrm{SO}}(\lambda_{jk})M(\lambda_{jk})}. \tag{4}$$

A detailed description of the determination of the responsivity and of the higher-order correction is given in [14,15].

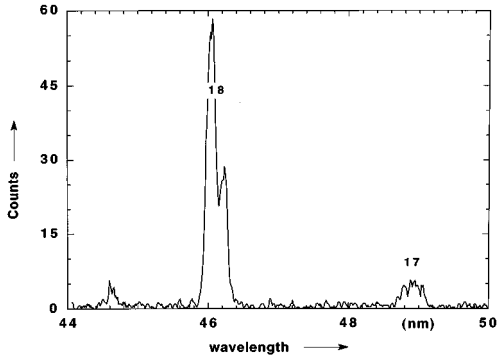

FIG. 1. vuv spectrum of electron-impact-induced line radiation of Ne in the wavelength range from 44 to 50 nm at 2-keV excitation energy. The feature numbers are listed in Table II with identifications and cross sections.

III. RESULTS

Fluorescence spectra for Ne, Ar, and Kr in the wavelength range between 44 and 100 nm with a resolution of 0.14 nm (full width at half maximum) are shown in Figs. 1–3. The spectra are not corrected for the variation of the responsivity of our spectrometer-detector system. The excitation energies are 2 and 3 keV, respectively. Compared with lower excitation energies, electrons at these energies are less sensitive to magnetic and electric stray fields and in our opinion have an advantage for radiometric applications.

From these spectra the numbered spectral lines, strong and well separated from their neighbors, were selected for the cross-section measurements. To avoid self-absorption effects, only ionic lines were chosen. Wavelengths and classifications of these lines are given in Tables I and II. Most of the Kr spectral lines were not considered in any cross-section measurement before. Due to the low count rates (10–100 counts/s, typically) we did not apply the scan mode for the

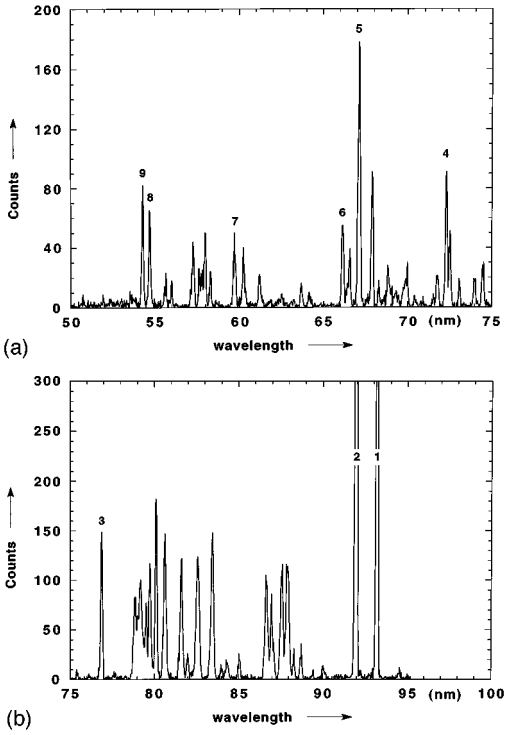

FIG. 2. vuv spectrum of electron-impact-induced line radiation of Ar in the wavelength range from 50 to 75 nm (a) and 75 to 100 nm (b) at 3-keV excitation energy. The feature numbers are listed in Table I with identifications and cross sections.

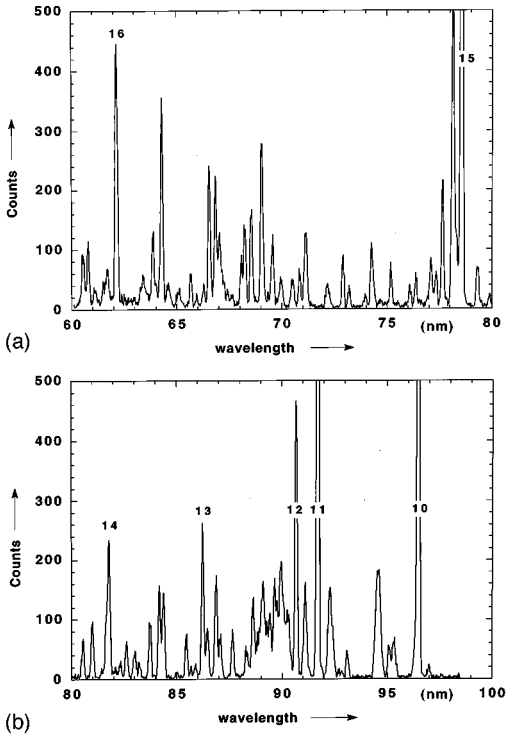

FIG. 3. vuv spectrum of electron-impact-induced line radiation of Kr in the wavelength range from 60 to 80 nm (a) and 80 to 100 nm (b) at 2-keV excitation energy. The feature numbers are listed in Table II with identifications and cross sections.

cross-section measurement. A monochromator exit slit width equivalent to a spectral bandwidth $\Delta\lambda$ of 0.4 nm was chosen to ensure that the complete spectral line was detected.

The apparent cross sections $\sigma_\perp(\lambda_{jk},E)$ determined for the electron-impact-induced fluorescence at excitation energies of 2 and 3 keV are given in columns 5 and 6, respectively, of Tables I and II. The total relative uncertainties $\Delta\sigma_\perp(\lambda_{jk},E)/\sigma_\perp(\lambda_{jk},E)$ of these data are given in column 7 of Tables I and II, which allow one to calculate the total absolute uncertainties $\Delta\sigma(\lambda_{jk},E)$. The contributions to the total uncertainties due to the uncertainties of the determinations of the number i/e of exciting electrons, the observed length ℓ of the electron beam, the target gas density n, the excitation energy E, and the radiant flux $\Phi^{\mathrm{SO}}(\lambda_{jk})$ emitted per second into a solid angle Ω have been discussed in detail [5] for the example of the Ar II $3s3p^6\ ^2S_{1/2}-3s^23p^5\ ^2P_{3/2}$ transition at 91.98 nm for 2-keV electron impact energy. Two of the uncertainties discussed in [5] change significantly towards lower wavelengths: below 57 nm, no higher-order correction is necessary to determine the spectral responsivity $\overline{s(\lambda)}$ of the monochromator-detector system; on the other hand, the uncertainty due to the monochromator wavelength calibration rises significantly, because the spectral responsivity varies considerably between 40 and 60 nm [14].

For some of the lines examined in this work, additional sources of uncertainty have to be considered: (1) The spectra shown in Figs. 1–3 were used to estimate additional relative uncertainties for the emission cross sections of lines 6, 11, 12, and 14–16 in the order of 0.6%–2.3% due to the tails of neighboring spectral lines. (2) Lines 10 and 13 may contain contributions of weak Kr I transitions. During the measurements of the ionic lines we used a target gas pressure of 7×10^{-4} mbar. To avoid self-absorption of the Kr I contribution in the measurement of line 10, a low pressure of 7×10^{-6} mbar was chosen. This was not possible for line 13 owing to its low intensity. Additional relative uncertainties of 0.6% and 3% for lines 10 and 13, respectively, result. (3) During the evaluation of our data we assumed unpolarized emission for all spectral lines, i.e., $P^{\mathrm{SO}}(\lambda_{jk})=0$, and used the responsivity $\overline{s(\lambda_{jk})}$ for unpolarized radiation [Eq. (4)]. Therefore, an additional contribution to the relative uncertainty of the radiant flux $\Phi^{\mathrm{SO}}(\lambda_{jk})$ and hence of the apparent cross section $\sigma_\perp(\lambda_{jk},E)$ has to be considered. From SR measurements in 0° and 90° orientation of the spectrometer-detector system, the polarization property $M(\lambda)$ of the system [Eq. (3)] was found to be less than 5% in the wavelength range from 40 to 120 nm. For Ar II lines 5 to 6 and Ar III line 3 we found the signal ratio of measurements in 0° and 90° orientation to be equal to 1, with a relative uncertainty of 1%, i.e., $P^{\mathrm{SO}}(\lambda_{jk})=0$ and $|P^{\mathrm{SO}}(\lambda_{jk})|\leqslant 20\%$. We assume the same for the Ne III, Kr II, and Kr III transitions. Since the product of MP^{SO} ($\leqslant 1\%$) determines the influence of polarization effects [Eq. (4)] a maximum systematic uncertainty of 1% for lines 3, 5–6, and 13–17 can arise.

IV. DISCUSSION

A. The rare gas $nsnp^6$-ns^2np^5 transitions

The heavier rare gases provide prominent line emission due to the $nsnp^6\ ^2S_{1/2}$-$ns^2np^5\ ^2P_{1/2,3/2}$ ionic transitions following the ns-electron ionization, where $n=2$, 3, and 4 for

TABLE I. Ar apparent photoemission cross sections $\sigma_\perp(\lambda_{jk},E)$ and their relative uncertainties $\Delta\sigma_\perp(\lambda_{jk},E)/\sigma_\perp(\lambda_{jk},E)$ for 2- and 3-keV excitation energy. Identifications according to [16].

Feature No.	Species	Transition	λ (nm)	$\sigma_\perp(\lambda_{jk},E)$ $E=2$ keV (10^{-20} cm^2)	$\sigma_\perp(\lambda_{jk},E)$ $E=3$ keV (10^{-20} cm^2)	$\Delta\sigma_\perp/\sigma_\perp$ (%)
Ar						
1	Ar II	$3p^6\ ^2S_{1/2}-3p^5\ ^2P_{1/2}$	93.21	57.0	40.9	2.8
2	Ar II	$3p^6\ ^2S_{1/2}-3p^5\ ^2P_{3/2}$	91.98	117	83.0	2.7
3	Ar III	$3p^5\ ^1P_1-3p^4\ ^1D_2$	76.92	10.4	8.2	2.9
4	Ar II	$(^3P)4s\ ^2P_{1/2}-3p^5\ ^2P_{1/2}$	72.56	13.6	8.9	2.7
	Ar II	$(^3P)4s\ ^2P_{3/2}-3p^5\ ^2P_{3/2}$	72.34			
5	Ar II	$(^1D)4s\ ^2D_{3/2}-3p^5\ ^2P_{3/2}$	67.29	16.1	10.9	2.6
		$(^1D)4s\ ^2D_{5/2}-3p^5\ ^2P_{3/2}$	67.19			
	Ar II	$(^3P)3d\ ^2D_{3/2}-3p^5\ ^2P_{1/2}$	67.09			
6	Ar II	$(^3P)3d\ ^2D_{5/2}-3p^5\ ^2P_{3/2}$	66.19	4.9		3.5
7	Ar II	$(^1S)4s\ ^2S_{1/2}-3p^5\ ^2P_{3/2}$	59.77	4.8	3.2	3.2
8	Ar II	$(^3P)5s\ ^4P_{3/2}-3p^5\ ^2P_{3/2}$	54.88	13.1	9.2	2.9
	Ar II	$(^3P)5s\ ^2P_{1/2}-3p^5\ ^2P_{1/2}$	54.80			
	Ar II	$(^1D)3d\ ^2S_{1/2}-3p^5\ ^2P_{1/2}$	54.75			
	Ar II	$(^3P)4d\ ^4D_{1/2}-3p^5\ ^2P_{1/2}$	54.72			
9	Ar II	$(^3P)5s\ ^2P_{1/2}-3p^5\ ^2P_{3/2}$	54.37	18.2	12.6	3.0
	Ar II	$(^3P)4d\ ^4D_{3/2}-3p^5\ ^2P_{3/2}$	54.35			
	Ar II	$(^1D)3d\ ^2S_{1/2}-3p^5\ ^2P_{3/2}$	54.32			
	Ar II	$(^3P)4d\ ^4D_{1/2}-3p^5\ ^2P_{3/2}$	54.29			

Ne, Ar, and Kr, respectively. The wavelengths of these ionic lines are Ne II: 46.1 and 46.2 nm; Ar II: 92.0 and 93.2 nm; and Kr II: 91.7 and 96.5 nm. In Figs. 4, 5, and 6, we compare the sum of our emission cross sections for Ne II: $[\sigma(46.1\ \text{nm})+\sigma(46.2\ \text{nm})]$, Ar II: $[\sigma(92.0\ \text{nm})+\sigma(93.2\ \text{nm})]$, and Kr II: $[\sigma(91.7\ \text{nm})+\sigma(96.5\ \text{nm})]$ at 2-keV excitation energy with the experimental data available [17–30]. In Figs. 7 and 8, we compare the experimental data with theoretical data for the ionization of the Ne $2s$ and the Ar $3s$ electron [31–38]. The comparison of the latter data will be discussed in Sec. IV C. The emission cross sections for the single lines are of interest for radiometric application, while the excitation cross sections for the ns subshells are more interesting from the viewpoint of the calculations.

In Figs. 4, 5, and 6, the published experimental cross sections for low excitation energies are scaled to 2-keV excitation energy using the mean of cross-section ratios, which are deduced from energy dependences obtained by measurement (Ne [17,19], Ar [17,23,27], Kr [17]). The ratios for the energies of interest agree with each other within $\pm 7\%$ and $\pm 4\%$ for Ne and Ar, respectively. Published cross-section values that are based on the cross section for Lyman-α emission following the electron-impact-induced dissociation of H_2 are renormalized to the cross-section value of 7.3×10^{-18} cm^2 for the Lyman-α emission at 100-eV excitation energy as suggested by van der Burgt *et al.* [9]. The figures show the uncertainties stated in the original publications; i.e., no uncertainties due to scaling and renormalization have been added.

For all gases we find large discrepancies of the experimental data available (some of them outside the reported uncertainties), in spite of the considerable efforts made in these experiments. To circumvent the problems of absolute cross-section measurements, especially the determination of the responsivity of the spectrometer-detector system, almost all published cross sections are based on relative measurements combined with normalization procedures. In many cases, results from the calculations of the first Born or Bethe approximation were used either directly or indirectly. For the comparison of the different techniques applied in the measurements and for the normalization, we refer to the original works and to the review by van der Burgt *et al.* [9]. The discrepancies of the data available show the problem of relative measurements and demonstrate the need for a set of reliable emission cross sections based on absolute measurements.

We find excellent agreement of the sum of our cross sections for Ar II $[\sigma(92.0\ \text{nm})+\sigma(93.2\ \text{nm})]$ with the value determined by the Risley group [10], which performed the only complete absolute measurement before. This group

TABLE II. Ne and Kr apparent photoemission cross sections $\sigma_\perp(\lambda_{jk},E)$ and their relative uncertainties $\Delta\sigma_\perp(\lambda_{jk},E)/\sigma_\perp(\lambda_{jk},E)$ for 2- and 3-keV excitation energy. Identifications according to [16].

Feature No.	Species	Transition	λ (nm)	$\sigma_\perp(\lambda_{jk},E)$ $E=2$ keV (10^{-20} cm^2)	$\sigma_\perp(\lambda_{jk},E)$ $E=3$ keV (10^{-20} cm^2)	$\Delta\sigma_\perp/\sigma_\perp$ (%)
Kr						
10	Kr II	$4p^6\ ^2S_{1/2}-4p^5\ ^2P_{1/2}$	96.50	99.5	70.7	2.9
	Kr I	$(^2P_{3/2})5d\ [\frac{3}{2}]_1-4p^6\ ^1S_0$	96.34			
11	Kr II	$4p^6\ ^2S_{1/2}-4p^5\ ^2P_{3/2}$	91.74	79.7	55.4	2.7
12	Kr III	$4s^0\ ^1S_0-4p^5\ ^1P_1$	90.71	28.9	23.0	3.2
13	Kr II	$(^3P)4d\ ^4D_{3/2}-3p^5\ ^2P_{1/2}$	86.48	18.9	13.8	4.0
	Kr I	$(^2P_{1/2})8d\ [\frac{3}{2}]_1-4p^6\ ^1S_0$	86.28			
	Kr III	$4p^5\ ^3P_2-4p^4\ ^3P_2$	86.26			
14	Kr II	$(^1D)5s\ ^2D_{3/2}-3p^5\ ^2P_{1/2}$	81.81	17.2	11.8	3.4
	Kr IV	$4p^4\ ^4P_{3/2}-4p^3\ ^4S_{3/2}$	81.68			
15	Kr III	$4p^5\ ^1P_1-4p^4\ ^1D_2$	78.60	80.1	64.5	3.7
16	Kr II	$(^1D)4d\ ^2S_{1/2}-4p^5\ ^2P_{3/2}$	62.19	23.9	16.4	2.9
	Kr III	$(^2D)4d\ ^1D_2-4p^4\ ^3P_1$	62.15			
	Kr II	$(^1S)4d\ ^2D_{5/2}-4p^5\ ^2P_{3/2}$	62.11			
Ne :						
17	Ne III	$2p^5\ ^3P_{2,1,0}-2p^4\ ^3P_{2,1,0}$	49.00	6.1	3.9	5.0
18	Ne II	$2p^6\ ^2S_{1/2}-2p^5\ ^2P_{1/2}$	46.24	11.4	83.0	3.9
	Ne II	$2p^6\ ^2S_{1/2}-2p^5\ ^2P_{3/2}$	46.07			

used the SURF II electron storage ring as the primary standard source in the vuv to determine the responsivity of the spectrometer-detector system used for the cross-section measurements. The differences of the two studies are discussed in [5]. Unfortunately, the work done by the Risley group was limited to the determination of the emission cross sections for the Ar II 92.0- and 93.2-nm transitions [10] and for the Lyman-α transition at 121.6 nm following the electron-impact-induced dissociation of H_2 [12]. In contrast, the set of

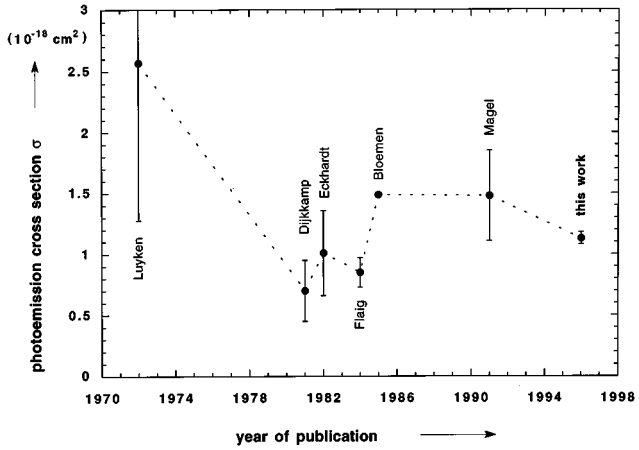

FIG. 4. Comparison of experimental data for the sum of the Ne II emission cross sections $[\sigma(46.2\text{ nm})+\sigma(46.1\text{ nm})]$ at 2-keV excitation energy: Luyken *et al.* [17], Dijkkamp and de Heer [18], Eckhardt and Schartner [19], Flaig [20], Bloemen [21], Magel [22].

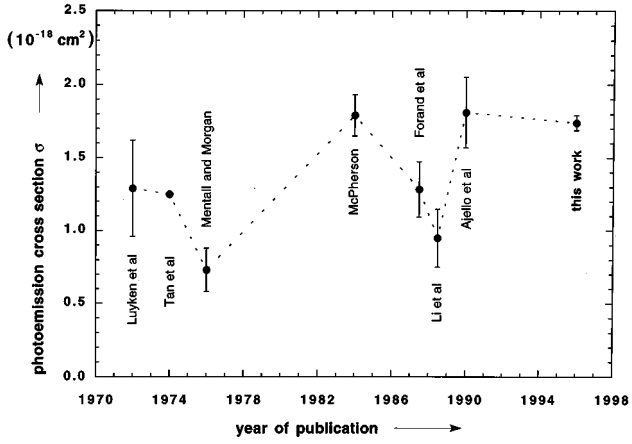

FIG. 5. Comparison of experimental data for the sum of the Ar II emission cross sections $[\sigma(92.0\text{ nm})+\sigma(93.2\text{ nm})]$ at 2-keV excitation energy: Luyken *et al.* [17], Tan and McConkey [23], Mentall and Morgan [24], McPherson [10], Forand *et al* [25], Li *et al.* [26], Ajello *et al.* [27].

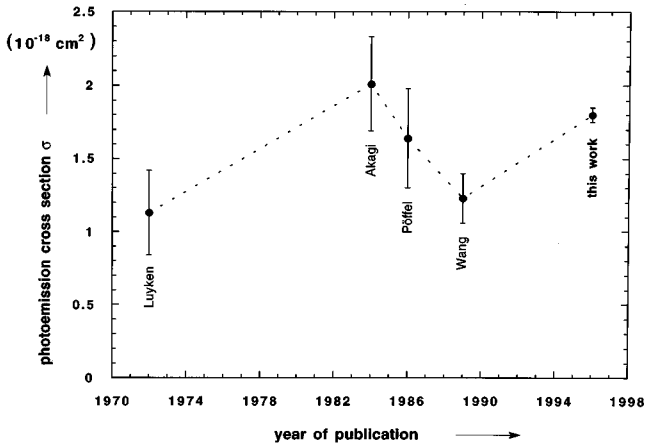

FIG. 6. Comparison of experimental data for the sum of the Kr II emission cross sections $[\sigma(91.7\text{ nm})+\sigma(96.5\text{ nm})]$ at 2-keV excitation energy: Luyken *et al.* [17], Akagi *et al.* [28], Pöffel [29], Wang *et al.* [30].

18 emission cross sections presented here covers the spectral range between 46 and 100 nm.

Moreover, we find excellent agreement of the sum of our cross sections for Ar II $[\sigma(92.0\text{ nm})+\sigma(93.2\text{ nm})]$ emission with the value recently determined by the Ajello group [27]. This agreement is surprisingly good since their value was obtained by a relative calibration technique based on the molecular H_2 excitation [7] and an absolute calibration using the emission cross section for the N I 120-nm emission following the electron-impact-induced dissociation of N_2 [39]. The latter cross section was determined by comparison with the emission cross section for the H I 121.6-nm emission [40] following the electron-impact-induced dissociation of H_2,

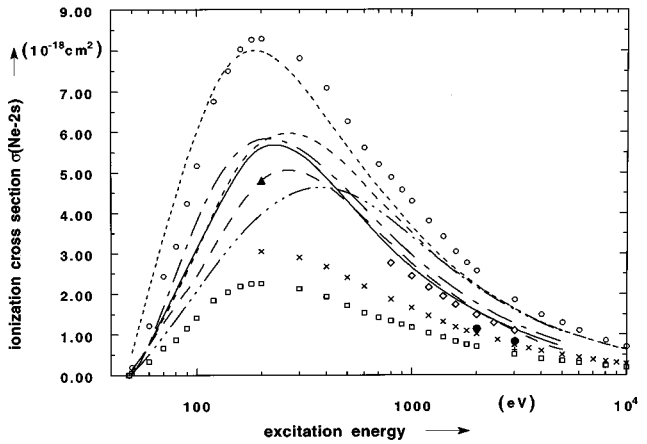

FIG. 7. Comparison of experimental data for the sum of the Ne II emission cross sections $[\sigma(46.1\text{ nm})+\sigma(46.2\text{ nm})]$ and the data calculated for the ionization cross section of an Ne 2*s* electron from threshold to 10 keV: Experiment: ○: Luyken *et al.* [17]; □: Dijkkamp and de Heer [18]; ×: Eckhardt and Schartner [19]; +; Flaig [20]; ▲: Bloemen [21]; ◇: Magel [22]; ●: this work. Theory: semiempirical: – - - - (Lotz [31]). – - – (Deutsch and Märk [35]); Born approximation: – – (Knapp and Schulz [32]), - - - (Wallace *et al.* [33]), — (McGuire [34]); Eikonal approximation: - - - (Wallace *et al.* [33]).

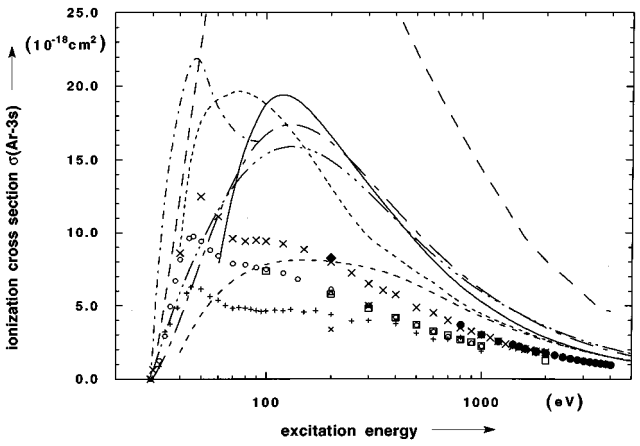

FIG. 8. Comparison of experimental data for the sum of the Ar II emission cross sections $[\sigma(92.0\text{ nm})+\sigma(93.2\text{ nm})]$ and the data calculated for the ionization cross section of a Ar 3*s* electron from threshold to 4 keV. Experiment: ○: Luyken *et al.* [17]; □: Tan and McConkey [23]; ×: Mentall and Morgan [24]; ♦: McPherson [10]; △: Forand *et al.* [25]; +: Li *et al.* [26]; ×; Ajello *et al.* [27]; ●; this work. Theory: semiempirical: – - - - (Lotz [31]), – - – (Deutsch and Märk [35]); Born approximation: – – (Omidvar *et al.* [36]), - - - (Wallace *et al* [33]), —-(McGuire [34]); Eikonal approximation: - - - (Wallace *et al.* [33]); Hartree Fock approximation: – - – (Amusia and Sheinerman [37]).

and it was renormalized in [39] as mentioned at the beginning of this section.

In the case of Kr we find good agreement with Pöffel's data [29]. In fact, this value is based on relative measurements and on the aforementioned cross section for the Ar II 92.0-nm emission determined by the Risley group [10].

B. The weaker transitions

In addition to the strong $nsnp^6\ ^2S_{1/2}$-$ns^2np^5\ ^2P_{1/2,3/2}$ ionic transitions, we studied several weaker transitions to cover the spectral range from 46 to 100 nm. To data, none of these cross sections was determined using an electron storage ring as a primary radiation standard. Most of the lines have not been studied at 2-keV excitation energy before. A comparison with the data available is, therefore, possible only for the Ar II 54.3-nm and 54.7-nm emissions (Table III) and the Ne III 49-nm emission.

As in the case of the Ne II 46-nm emission, the cross sections for the Ne III 49-nm emission of Eckhardt and Schartner [19] and Flaig [20] are too low by approximately 13% compared with our result. Nevertheless, the emission cross-section ratios $\sigma(49\text{ nm})/\sigma(46\text{ nm})$ agree within 2%.

The Ar II $3s^23p^4(^1D)3d\ ^2S_{1/2}$-$3s^23p^5\ ^2P_{1/2,3/2}$ transitions at 54.3 and 54.7 nm were measured by Tan and McConkey [23] for excitation energies between threshold and 1 keV and by Ajello *et al.* [27] at 200-eV excitation energy. These data are scaled to 2-keV excitation energy using the energy dependence measured by Kraus [41]. The emission cross-section values of Tan and McConkey [23] and Ajello *et al.* [27] are in very good agreement with our measurements, whereas the value of Kraus [41] is too high by 26% at 2-keV excitation energy (Table III).

These transitions were received with considerable interest because the Ar II $3s3p^6\ ^2S_{1/2}$ state is strongly affected by

TABLE III. Comparison of Ar II $\sigma(3d')=\sigma(54.3\text{ nm})+\sigma(54.7\text{ nm})$ photoemission cross sections, cross-section ratios $\sigma(3d')/\sigma(3s)=[\sigma(54.3\text{ nm})+\sigma(54.7\text{ nm})]/[\sigma(92.0\text{ nm})+\sigma(93.2\text{ nm})]$ at 2-keV excitation energy, and spectroscopic factors calculated for the Ar II $3s3p^6$ state

	$\sigma(3d')$ (10^{-20} cm^2)	$\sigma(3d')/\sigma(3s)$ (%)	Spectroscopic factor ($3s3p^6$)
	Theory		
Luyken *et al.* (1972) [17]		50.0	0.62
Dyall and Larkins (1982) [42]		13.2	0.612
Smid and Hansen (1983) [43]		13.5	0.629
Mitroy *et al.* (1984) [44]		20.7	0.603
Amusia and Kheifets (1985) [45] for $(e,2e)$		36.4	0.55
for (γ, e)		18.8	0.79
Hibbert and Hansen (1987) [46]		18.1	0.618
Wijesundera and Kelly (1989) [47]		14.7	
Decleva *et al.* (1990) [48]		18.7	0.602
	Experiment		
Tan and McConkey (1974) [23] [a]	32.7	27.0	
Spears *et al.* (1974) [49] (γ,e)		18.8	
McCarthy and Weigold (1985) [50]$(e,2e)$		32.0	
Kraus (1986) [41] [a]	39.5	22.2	
Svensson *et al.* (1988) [51](γ,e)		18.6	
Ajello *et al.* (1990) [27] [a]	34.2	18.9	
This work[a]	31.4	18.1	

[a]Electron-impact-induced fluorescence spectroscopy.

configuration interaction with the Ar II $3s^23p^4(^1D)3d\ ^2S_{1/2}$ state. Table III compares the ratios for the emission cross sections $[\sigma(54.3\text{ nm})+\sigma(54.7\text{ nm})]/[\sigma(92\text{ nm})+\sigma(93.2\text{ nm})]$ determined in different experiments with the ratios calculated for the excitation cross sections $\sigma[\text{Ar II } 3s^23p^4(^1D)3d^2S_{1/2}]/\sigma(\text{Ar II}3s3p^6\ ^2S_{1/2})=\sigma(d')/\sigma(3s)$. We refer to Tan and McConkey [23], who showed that the excitation cross sections are represented by the emission cross sections, i.e., that contributions to the cross section due to cascades and nearby lines are neglible at higher excitation energies. We find good agreement of our cross-section ratio value with the value of Ajello *et al.* [27]. Our value supports the value recently determined by Svensson *et al.* [51] using x-ray photoelectron spectroscopy and the values calculated by Hibbert and Hansen [46] and Decleva *et al.* [48] both taking configuration interaction into account. Amusia und Kheifets [45] calculated different spectroscopic factors for (γ,e) and $(e,2e)$ experiments, leading to different cross-section ratios $\sigma(d')/\sigma(3s)$. Surprisingly, our value agrees with their ratio for (γ,e) experiments rather than with their ratio for $(e,2e)$ experiments.

C. Comparison of cross sections for the Ne and Ar *s*-shell ionization from threshold up to 4 keV

In Figs. 7 and 8, we compare the experimental and theoretical data available for Ne $2s$ and Ar $3s$ ionization from threshold up to 10- and 4-keV excitation energy, respectively. In the case of Ar $3s$ ionization (Fig. 8), we reduced all theoretical data by a factor of 0.61, the mean of the calculated spectroscopic factors listed in Table III. This was done to take into consideration the effect of the interaction between the Ar II $3s3p^6\ ^2S_{1/2}$ configuration and the Ar II $3s^23p^4(^1D)nd/\varepsilon d\ ^2S_{1/2}$ configurations. This effect is not taken into account in the calculations of electron-impact ionization cross sections, but its severe influence has been shown in the study of the photoionization of the Ar $3s$ electron ([52] and references therein). In the case of the Ne $2s$ ionization (Fig. 7), no corrections are applied to the theoretical data because configuration interaction is negligible [18].

Not surprisingly, the calculations within the Born approximation overestimate the cross sections at low excitation energies. But we find large discrepancies between our experimental data and the theoretical data even in the region of high excitation energies, where the Born approximation is expected to yield correct absolute ionization cross sections. The Born approximation was shown to correctly describe the high-energy dependence of the ionization cross section (e.g., [17]), but for the calculation of the correct absolute cross-section values appropriate wave functions are needed.

In the case of the Ar $3s$ electron ionization, the experimental results [17,26,27] indicate a maximum of the ionization cross section at about 20 eV above threshold. None but the calculations by Amusia and Sheinerman [37] within the Hartree-Fock approximation describe this feature. However, their absolute values are still too high by a factor of approximately 1.7, again indicating the need for improved cross-section calculations.

We mention in particular the discrepancies between our data and the results of Lotz [31] and Deutsch and Märk [35] for Ne and Ar. Both works develop simple semiempirical formulas that are of great interest to reduce the calculational efforts in complex plasma model calculations. However,

both calculations fail to describe the maximum of the cross section at low excitation energies, and their absolute values are by far too high at all excitation energies.

V. SUMMARY

We measured a set of 18 absolute cross sections for electron-impact-induced line radiation of Ne, Ar, and Kr in the spectral range between 46 and 100 nm, providing an accurate database for the use of an electron-impact excitation source as a source of calculable radiant flux. Unparalleled, low uncertainties were achieved, mainly because the electron storage ring BESSY served as a primary standard source in the vuv for the determination of the responsivity of the spectrometer-detector system and because a spinning rotor gauge was used as a secondary standard for the determination of the target gas density. Very good agreement with the most reliable experimental data [10] for the prominent Ar II $3s3p^6\ ^2S_{1/2}$-$3s^23p^5\ ^2P_{3/2,1/2}$ transitions at 92.0 and 93.2 nm was observed. Comparing our results with published experimental data based on relative measurements, and with theoretical data, we have found strong discrepancies that demonstrate the need for a set of reliable experimental emission cross sections traceable to a primary radiation standard as given in this work.

ACKNOWLEDGMENTS

The assistance of the NOKIA electronics company, who provided the electron guns used, is gratefully acknowledged. The work presented was funded by the Bundesminister für Forschung und Technologie under Contracts No. 05 5DBDAB 5 and No. 05 5RGAXB 3.

[1] F. Riehle and B. Wende, Metrologia **22**, 75 (1986).
[2] D. Arnold, G. Ulm, Rev. Sci. Instrum. **63**, 1539 (1992).
[3] M. L. Furst, R. M. Graves, L. R. Canfield, and R. E. Vest, Rev. Sci. Instrum. **66**, 2257 (1985).
[4] G. Ulm and B. Wende, Rev. Sci. Instrum. **66**, 2244 (1995).
[5] W. Jans, B. Möbus, G. Ulm, M. Kühne, A. Werner, and K.-H. Schartner, Appl. Opt. **34**, 3671 (1995).
[6] K.-H. Schartner, B. Kraus, W. Pöffel, and K. Reymann, Nucl. Instrum. Methods B **27**, 519 (1987).
[7] J. M. Ajello, D. E. Shemansky, B. Franklin, J. Watkins, S. Srivastava, G. K. James, W. T. Simms, C. W. Hord, W. Pryor, W. McClintock, V. Arabright, and D. Hall, Appl. Opt. **27**, 890 (1988).
[8] J. S. Risley and W. B. Westerveld, Appl. Opt. **28**, 389 (1989).
[9] P. J. M. van der Burgt, W. B. Westerveld, and J. S. Risley, J. Phys. Chem. Ref. Data **18**, 1757 (1989).
[10] A. McPherson, Ph.D. thesis, North Carolina State University, Raleigh, NC, 1984 (unpublished).
[11] A. McPherson, N. Rouze, W. B. Westerveld, and J. S. Risley, Appl. Opt. **25**, 298 (1986).
[12] R. Ligtenberg, A. Graves, A. McPherson, N. Rouze, W. B. Westerveld, and J. S. Risley, EOS Trans. AGU **66**, 993 (1985).
[13] W. Jans, Ph.D. thesis, Technische Universität Berlin (1993).
[14] J. Hollandt, W. Jans, M. Kühne, F. Lindenlauf, and B. Wende, Rev. Sci. Instrum. **63**, 1278 (1992).
[15] J. Hollandt, M. Kühne, and B. Wende, Appl. Opt. **33**, 68 (1994).
[16] R. L. Kelly, J. Phys. Chem. Ref. Data **16**, Suppl. 1 (1987).
[17] B. F. J. Luyken, F. J. de Heer, and R. Ch. Baas, Physica **61**, 200 (1972).
[18] D. Dijkkamp, and F. J. de Heer, J. Phys. B **14**, 1327 (1981).
[19] M. Eckhardt and K.-H. Schartner, Z. Phys. A **312**, 321 (1983).
[20] H.-J. Flaig, Ph.D. thesis, Gieβen University, 1984.
[21] E. W. P. Bloemen, in Ph.D. thesis of D. Dijkkamp, University of Utrecht, 1985.
[22] B. Magel, Diploma thesis, Gieβen University, 1991 (unublished).
[23] K.-H. Tan and J. W. McConkey, Phys. Rev. A **10**, 1212 (1974).
[24] J. E. Mentall and H. D. Morgan, Phys. Rev. A **14**, 954 (1976).
[25] J. L. Forand, S. Wang, J. M. Woosley, and J. W. McConkey, Can. J. Phys. **66**, 349 (1988).
[26] G. P. Li, T. Takayanagi, K. Wakiya, and H. Suzuki, Phys. Rev. A **38**, 1831 (1988).
[27] J. M. Ajello, G. K. James, B. Franklin, and S. Howell, J. Phys. B **23**, 4355 (1990).
[28] Y. Akagi, M. Hayakawa, Y. Morikawa, T. Takayanagi, K. Wakiya, and H. Suzuki (unpublished).
[29] W. Pöffel, Diploma thesis, Gieβen University, 1986 (unpublished).
[30] S. Wang, P. J. M. van der Burgt, and J. W. McConkey, J. Phys. B **22**, L341 (1989).
[31] W. Lotz, Z. Phys. **206**, 205 (1967).
[32] E. W. Knapp and M. Schulz, J. Phys. B **7**, 1875 (1973).
[33] S. J. Wallace, R. A. Berg, and A. E. S. Green, Phys. Rev. A **7**, 1616 (1973).
[34] E. J. McGuire, Phys. Rev. A **16**, 73 (1977).
[35] H. Deutsch and T. D. Märk, Contrib Plasma Phys. **34**, 19 (1994).
[36] K. Omidvar, H. L. Kyle, and E. C. Sullivan, Phys. Rev. A **5**, 1174 (1972).
[37] M. Ya Amusia and S. A. Sheinerman, J. Phys. B **12**, 649 (1979).
[38] K. Bartschat and P. G. Burke, J. Phys. B **21**, 2969 (1988).
[39] J. M. Ajello, G. K. James, B. O. Franklin, and D. E. Shemansky, Phys. Rev. A **40**, 3524 (1989).
[40] J. M. Ajello and D. E. Shemansky, J. Geophys. Res. **90**, 9845 (1985).
[41] B. Kraus, Diploma Thesis, Gieβen University, 1986 (unpublished).
[42] K. G. Dyall and F. P. Larkins, J. Phys. B **15**, 203 (1982).
[43] H. Smid and J. E. Hansen, J. Phys. B. **16**, 3339 (1983).
[44] J. Mitroy, K. Amos, and I. Morrison, J. Phys. B **17**, 1659 (1984).
[45] M. Ya Amusia and A. S. Kheifets, J. Phys. B **18**, L679 (1985).
[46] A. Hibbert and J. E. Hansen, J. Phys. B **20**, L245 (1987).
[47] W. Wijesundera and H. Kelly, Phys. Rev. A **39**, 634 (1989).
[48] P. Decleva, G. De Alti, G. Fronzoni, and A. Lisini, J. Phys. B **23**, 3777 (1990).

[49] D. P. Spears, H. J. Fishbeck, and T. A. Carlson, Phys. Rev. A **9**, 1603 (1974).
[50] I. E. McCarthy and E. Weigold, Phys. Rep. **27**, 275 (1976).
[51] S. Svensson, B. Eriksson, N. Martensson, G. Wendin, and U. Gelius, J. Electron Spectrosc. **47**, 327 (1988).
[52] B. Möbus, B. Magel, K.-H. Schartner, B. Langer, U. Becker, M. Wildberger, and H. Schmoranzer, Phys. Rev. A **47**, 3888 (1993).